Research Repository UCD

Provided by the author(s) and University College Dublin Library in accordance with publisher policies. Please cite the published version when available.

Title	Achieving enhanced DSSC performance by microwave plasma incorporation of carbon into TiO2 photoelectrodes
Author(s)	Dang, Binh H.Q.; MacElroy, J. M. Don; Dowling, Denis P.
Publication date	2013-06-15
Publication information	Applied Surface Science, 275 (15 June 2013): 289-294
Publisher	Elsevier
Item record/more information	http://hdl.handle.net/10197/4199
Publisher's statement	This is the author's version of a work that was accepted for publication in Applied Surface Science. Changes resulting from the publishing process, such as peer review, editing, corrections, structural formatting, and other quality control mechanisms may not be reflected in this document. Changes may have been made to this work since it was submitted for publication. A definitive version was subsequently published in Applied Surface Science (Volume 275, 15 June 2013, Pages 289–294). DOI:10.1016/j.apsusc.2012.12.121 Elsevier B.V.
Publisher's version (DOI)	http://dx.doi.org/10.1016/j.apsusc.2012.12.121

Downloaded 2018-03-19T20:57:31Z

The UCD community has made this article openly available. Please share how this access benefits you. Your story matters! (@ucd_oa)

Some rights reserved. For more information, please see the item record link above.


BY NC ND

Achieving enhanced DSSC performance by microwave plasma incorporation of carbon into TiO_2 photoelectrodes

Binh H. Q. Dang [1], Don MacElroy [1], Denis P. Dowling [1,2,*]

[1] School of Chemical & Bioprocess Engineering, University College Dublin, Ireland

[2] School of Mechanical & Materials Engineering, University College Dublin, Ireland

* Corresponding author,

Dr. Denis P. Dowling

Room 223, UCD Engineering & Materials Science Center,

University College Dublin, Belfield, Dublin 4, Republic of Ireland

Tel: (+353) 1 716 1747

Fax: (+353) 1 283 0534

E-mail: denis.dowling@ucd.ie

Abstract

The photoactivity of carbon-incorporated titanium dioxide (TiO_2) has been widely reported. This study involves a novel approach to the incorporation of carbon into TiO_2 through the use of microwave plasma processing. The process involved thermally treating printed TiO_2 nanoparticle coatings in a microwave-induced argon-oxygen plasma containing low concentrations of methane. The resulting deposited carbon layer was characterized using XRD, XPS, Raman, UV-VIS, ellipsometry, and optical profilometry. It was found that methane gas had been dissociated in the microwave plasma into carbon species, which were then deposited as a nm-thick layer onto the TiO_2 coatings, most likely in the form of graphite. The photovoltaic performances of both the TiO_2 and the carbon-incorporated TiO_2 were assessed through *J-V* and IPCE measurements of the N719-sensitized solar cells using the titania as their photoanodes. Up to a 72% improvement in the maximum power density ($P_{d\text{-}max}$) was observed for the carbon-incorporated TiO_2 samples as compared to the TiO_2, onto which no carbon was added. This improvement was found to be mainly associated with an increase in the short-circuit current density (J_{sc}), but independent from the open-circuit voltage (V_{oc}), the filter factor (*FF*), and the level of dye adsorption. Possible contributory factors to the improved performance of the carbon-incorporated TiO_2 were the enhanced electron conductivity and electron lifetime, both of which were elucidated through electrochemical impedance spectroscopy (EIS). When the surface layer was examined using XPS, the optimal carbon content on the TiO_2 coating surface was found to be 8.4%, beyond which there was a reduction in the DSSC efficiency.

Key words: microwave plasma, carbon incorporation, titanium dioxide, dye-sensitized solar cells

1. Introduction

Dye-sensitized solar cells (DSSCs) have attracted considerable attention as a promising alternative to traditional silicon-based solar cells due to their low fabrication costs and yet relatively high solar energy conversion efficiency even in diffuse light [1-4]. There has been a large number of reports on techniques that can enhance both DSSC efficiency and stability; one method of which is to introduce novel materials as charge carriers into the cells to facilitate the photogenerated charge transport, therefore overcoming charge recombination [5-10]. Among such materials, various carbon structures have recently been investigated owing to their high electrical conductivity and hence ability to reduce the charge transfer resistance within the cells, thus improving the overall charge transfer efficiency. Tsai et al. spin-coated graphene-TiO_2 composite pastes onto ITO to use as the photoanodes in DSSCs and reported a 15% improvement in the cell efficiency [11]. Using a modified Hummers method followed by chemical reducing and annealing, Yang et al. introduced graphene as 2D-bridges into the TiO_2 photoanodes, leading to faster electron transport and lower recombination; this yielded a 39% increase in the efficiency of their DSSCs [12]. In another work, Jang et al. fabricated ordered arrays of TiO_2 dots embedded in carbon matrix via UV-stabilization of polystyrene-*block*-poly(4-vinylpyridine) films containing TiO_2 precursors followed by direct carbonization [13]. They then applied these graphite-TiO_2 thin films onto the external surface of TiO_2-coated photoanodes and observed a 40.6% increase in the power conversion efficiency of the resulting DSSCs. In this paper, the use of a microwave plasma as a processing technique for incorporating carbon into TiO_2 nanoparticle photoanodes is evaluated for the first time. The process involved thermally treating printed TiO_2 coatings in a microwave-induced argon-oxygen plasma containing low concentrations of methane. Methane has been widely reported as a precursor for the plasma deposition of diamond

and graphitic films [14-16]. Microwave (MW) plasmas have also been used previously for the sintering of metal oxide nanoparticles such as NiO_x and TiO_2 for use in solar devices [17, 18]. The MW-induced argon-oxygen plasma treatments were demonstrated to be both more time- and energy-efficient compared with conventional furnace sintering. When used as the photoanodes in DSSCs, the resulting sintered nanoparticle coatings were also found to have better photovoltaic performance, as the MW plasma sintering promotes better interface adhesion between the coatings and the substrates.

2. Experimental procedures

2.1. Screen-printing of TiO_2 photoanodes – Fluorine-doped tin oxide (FTO) glass slides supplied by Pilkington Glass were used as the conducting substrates. They were first ultrasonically cleaned in isopropanol for 15 min and then dried in an oven at 150 ˚C for a further 15 min. The FTO glass substrates were subsequently immersed in a solution of 40 mM titanium tetrachloride ($TiCl_4$) in de-ionized water for 30 min at 70 ˚C, so as to deposit a thin compact layer of TiO_2 onto FTO [19-23]. The substrates were then dried in an oven for another 30 min. A deposition paste was supplied by Dyesol, comprising of TiO_2 nanoparticles of size ~ 20 nm suspended in a dispersion medium. An absorption layer of ~ 3 μm (1 pass) was deposited onto the FTO glass substrates by a Digitek screen-printer using this paste. The printed glass slides were then placed in a drying box for 15 min. Another deposition paste was obtained from Dyesol, comprising of TiO_2 nanoparticles of size ~ 400 nm suspended in a dispersion medium. A scattering layer of ~ 6 μm (2 passes) was screen-printed on top of the absorbing layer using this paste. The printed glass slides were finally cut into small 2 x 3 cm^2 working electrodes that contained 1 x 1 cm^2 of TiO_2 prints.

2.2. Microwave plasma processing and DSSC assembly – The TiO_2-coated FTO glass substrates were thermally treated using a circumferential antenna plasma (CAP) MW (2.45 GHz) system, which has been described elsewhere [24-26]. The chamber was first pumped down to 8 Pa at which point 10 sccm of oxygen (99.9%) and 50 sccm of argon (99.998%) were introduced into the chamber. The total gas pressure was then adjusted to 800 Pa using a manual throttle valve and a microwave discharge was ignited to form a plasma ball around the samples located in the center of the chamber. Substrate temperatures were monitored using a LASCON QP003 two-color pyrometer from Dr. Mergenthaler GmbH & Co. Input powers of 2.4 kW were provided from a Mugge microwave power supply. The samples were treated at 550 ˚C for 15 min; these were the plasma gas conditions used for sintering TiO_2. The incorporation of carbon into the TiO_2 was achieved by introducing a low concentration of methane (99.995%) into the argon-oxygen gas mixture during the sintering process. A methane flow rate in the range of 0.5 to 3.5 sccm was investigated and the chamber pressure was maintained at 800 Pa. Both the TiO_2 prints sintered with and without the addition of methane were then sensitized with 0.3 mM N719 dye in a 99.8% ethanol solution for 24 hours. The DSSCs were finally assembled using the prepared TiO_2 as their photoanodes and platinum-coated FTO glasses as their photocathodes with an iodide/tri-iodide-based solution as the electrolyte.

2.3. Characterization techniques – The crystalline phase composition of the samples was examined by a Siemens D500 X-ray diffractometer (XRD) operating at 40 kV and 30 mA with Cu Kα radiation at a wavelength of 0.1542 nm. The scan was in 2θ mode and spanned from 20˚ to 70˚ with steps of 0.02˚ per second. X-ray photoelectron spectroscopy (XPS) analysis of the samples was carried out using a Kratos AXIS 165 spectrometer with a monochromatic Al Kα radiation ($h\nu$ = 1486.58 eV). The print thickness was obtained through step height measurements

using a WYKO NT1100 optical profilometer in vertical scanning interferometry (VSI) mode. Room temperature micro-Raman scattering spectra were obtained using a SENTERRA dispersive Raman microscope from Bruker Optics. The samples were excited with 785 nm line of a DPSS laser, focused to ~ 1 μm by using microscope objective lens (x 20). Dye adsorption levels were obtained indirectly through UV-VIS measurements of desorbed dye molecules in 0.1 M NaOH. Incident monochromatic photo-to-current conversion efficiency (IPCE) performance of the photoanodes was measured by illumination with monochromatic lights in the rage of 300 – 800 nm, which were attained through a monochromator and an order sorting filter. The *J-V* characteristics of the prepared DSSCs were studied under 200 lux to stimulate diffuse indoor lighting conditions. Electron transport properties were investigated using electrochemical impedance spectroscopy (EIS) with measurements at open-circuit voltage under the illumination of one sun.

3. Results and discussion

The overall objective of this study is to determine the effect of methane addition during the MW plasma sintering of TiO_2 nanoparticles for use in DSSCs. This results section is divided into two parts; the first deals with the characterizations of the MW plasma-sintered TiO_2 with and without the addition of methane during the sintering process. The second part presents results on the photovoltaic performance of the DSSCs fabricated using these TiO_2 coatings as their photoanodes. The photovoltaic performance of the TiO_2 coatings sintered with and without the presence of methane at different flow rates was compared against each other. DSSCs are particularly known for their superior performance under low and diffuse light; as a result, *J-V* measurements were carried out under 200 lux to stimulate indoor lighting conditions instead of the commonly tested AM 1.5 illumination.

3.1. Characterizations of the TiO_2 working electrodes

Fig. 1 shows the XRD spectra of both an uncoated and a TiO_2-coated FTO glass samples, which were sintered with the addition of methane (3.5 sccm) during the MW plasma treatment process. Characteristic peaks indexed in the graph correspond to anatase TiO_2. Similar peaks were also found in the XRD spectra of the TiO_2 coatings treated with and without methane at other flow rates (0.5 – 3.0 sccm). This study indicates that the addition of methane under the plasma processing conditions used did not alter the TiO_2 crystalline phase composition.

The Raman spectra of coatings such as that obtained for the sample sintered in the presence of 3.5 sccm of methane (Fig. 2) also demonstrated the presence of anatase TiO_2 in the coatings, independently on whether they had been sintered with or without the addition of methane. In the case of the TiO_2 coatings sintered in the presence of methane however, there is evidence for the presence of carbon as indicated by the presence of the *D* band at approximately 1350 cm^{-1} as shown in Fig. 3. It is important to note however that the corresponding *G* band expected for carbon structures in the range of 1580 – 1600 cm^{-1} was extremely weak [13]. According to Ferrari et al., a high I(*D*)/I(*G*) intensity ratio indicates that the carbon layer has only sp^2-hybridized (graphite-like) bonding and no sp^3-hybridized (diamond-like) character [27]. Given that these bands were only found in the TiO_2 coatings which had been MW plasma-sintered in the presence of methane, it is reasonable to assume that methane had been dissociated in the MW plasma to carbon species which were then deposited onto TiO_2, mostly likely in the form of graphite.

XPS analysis was carried out to investigate the effect of methane addition at different flow rates on the sintered coatings. Fig. 4 shows a typical XPS spectrum for the C1s state with

the deconvoluted peak at 284.7 eV representing C–C inorganic carbon, while the other peaks representing organic carbons [28]. This C–C peak is absent in the case of the TiO_2 coating that was MW plasma-sintered without the addition of methane. The coatings MW-plasma sintered in the presence of methane also had their outer layer removed by argon sputtering and the C–C peak was found to be absent in their XPS spectra as well. This indicates that the methane-deposited carbon did not diffuse significantly into the TiO_2 coating bulk. The corresponding percentage carbon (%C) of the coatings sintered in the presence of methane (0.5 – 3.5 sccm) is plotted in Fig. 5. As shown in this figure, the amount of deposited carbon (%C) is found to increase with increasing methane flow rates ~~in~~ used during the MW plasma sintering process. In order to determine the thickness of the carbon layer, spectroscopic ellipsometry was used. Measurements were obtained with a Woollam M-2000 variable wavelength ellipsometer on uncoated silicon substrates which had been placed in the MW plasma adjacent to the TiO_2 coatings. The ellipsometric data were recorded at incident angles of 65˚, 70˚ and 75˚, and the measurements were fitted to a three-phase model which consists of a Si substrate, a SiO_2 interfacial layer (fixed at 2 nm), and a fittable Cauchy carbon thin film. Also shown in Fig. 5, the thickness of the carbon layer on the flat silicon wafer surface was found to increase with increasing methane flow rate and a thickness of up to 7.0 nm was obtained at a methane flow rate of 3.5 sccm for the treatment time of 15 min.

3.2. Photovoltaic performances of DSSCs using carbon-incorporated TiO_2 photoanodes

Fig. 6 displays the maximum power densities ($P_{d\text{-}max}$) of the DSSCs prepared using TiO_2 and carbon-incorporated TiO_2 photoelectrodes (6.7 – 9.7 %C prepared using 0.5 – 3.5 sccm of precursor methane accordingly). This figure demonstrates that there is an overall increase in $P_{d\text{-}max}$ for DSSCs using carbon-incorporated TiO_2 photoanodes as compared to the coating sintered

in the absence of methane. Nonetheless, the value of $P_{d\text{-}max}$ only increases with increasing carbon content, measured at the TiO_2 surface by XPS, up to 8.4% (prepared using 2.5 sccm of methane). Above this concentration, the maximum power density values decreased. The corresponding $P_{d\text{-}max}$ values for the DSSCs using TiO_2 photoanodes sintered with and without 2.5 sccm of methane addition are 3.16 and 5.44 $\mu W/cm^2$ respectively, representing a 72% increase in the maximum power density. Such a significant enhancement in photovoltaic performance has previously been accounted for by an increase in the level of dye adsorption on TiO_2 [11]. In this current study however, a UV-VIS analysis indicates that there was in fact a decrease in the level of dye adsorption with an increase in the methane content used during the MW plasma sintering. Based on a desorption study [13], the concentration of loadable dyes was found to gradually decrease from 5.38×10^{-5} to 4.71×10^{-5} mM/cm^2 for the photoanodes that were prepared in the absence of methane and in the presence of up to 3.5 sccm of methane respectively (Fig. 6). This decrease in the dye adsorption level could be explained by an interruption of the dye loading process due to the carbon layer acting as a barrier on the surface of TiO_2 [13]. For TiO_2 layers with carbon content up to the optimal 8.4% (measured at the surface by XPS), the value of $P_{d\text{-}max}$ increases despite the small reduction in the level of adsorbed dye. This would indicate that there was another factor whose impact was high enough to compensate for this decrease in the level of dye adsorption.

The detailed current density – voltage (*J-V*) responses of TiO_2 and the carbon-incorporated TiO_2 were analyzed in order to investigate the effect of the carbon layer on the electrical properties of the coatings. Whereas the open-circuit voltage (V_{oc}) and the fill factor (*FF*) remain relatively constant with varying carbon content (Fig. 7), the short-circuit current density J_{sc} is found to fluctuate (Fig. 8). Given that the shape of the curve in Fig. 8 is similar to

that of Fig. 6, which plots $P_{d\text{-}max}$ against methane flow rate (hence carbon content), it is suggested that the observed change in $P_{d\text{-}max}$ values are mainly associated with changes in J_{sc}. In other words, J_{sc} and hence $P_{d\text{-}max}$ increase with increasing carbon content up to 8.4% when measured at the surface by XPS (layer thickness ~ 6.4 nm) and decrease thereafter. The same trend is also reflected in the IPCE performances. As illustrated in Fig. 9, the IPCE response is maximized at the wavelengths of 335 and 530 nm. Overall the IPCE responses at these two wavelengths as well as all the other wavelengths are enhanced for the carbon-incorporated TiO_2. This enhancement in IPCE is likely to be due to carbon in the form of graphite as it is a good electron carrier, which facilitates the photogenerated charge transport and suppresses the recombination and back reaction [13]. With higher carbon contents above the 8.4% measured at the surface, the excess carbon can act as a recombination center instead of providing an electron pathway, which means short circuit can happen more easily [12]. In this latter case, not only did carbon not offset the reduced level of dye adsorption at higher carbon content as previously discussed, but it also diminished J_{sc} and hence $P_{d\text{-}max}$ as shown in Fig. 8 and 6 respectively.

To obtain a greater understanding of the effect of carbon incorporation, the charge transport properties of the coatings were evaluated using EIS measurements on the TiO_2 as well as the best-performing 8.4% surface carbon-incorporated TiO_2 coatings. Fig. 10 presents the results using Nyquist plots with the three distinctive semicircles [11, 29, 30]. The first semicircle is attributed to the impedance of the charge transfer process at the counter electrode/electrolyte interface; the second semicircle is ascribed to the impedance of the charge transfer process at the working electrode/electrolyte interface; and the third semicircle is related to the Nernstian diffusion in the electrolyte. As shown in Fig. 10, the semicircles for the 8.4% surface carbon-incorporated TiO_2 are smaller than those of the TiO_2 only photoanode. This indicates a lower

interfacial charge transfer resistance and hence a higher charge transfer efficiency. These results can also be viewed using Bode plots as shown in Figure 11, which enables information to be extracted about the electron lifetime within the photoanodes [11, 29, 30]. These plots indicated electron lifetimes of approximately 14 milliseconds for the TiO_2 and 33 milliseconds for the 8.4% surface carbon-incorporated TiO_2. This increase is again likely to be due to the deposition of carbon in the form of graphite with its high electrical conductivity acting as carriers within the cell, thus helping to facilitate the charge transport and restraining charge recombination.

4. Conclusions

Carbon-incorporated TiO_2 photoanodes were successfully prepared during the sintering of TiO_2 coatings using a MW argon-oxygen-methane plasma. Based on XPS analysis, the deposited carbon is concentrated on the surface of the TiO_2 coatings and not in the bulk. The carbon-incorporated TiO_2 demonstrated a higher photovoltaic performance compared to the TiO_2 only coating, when used as photoanodes in DSSC applications. Up to a 72% increase in maximum power density $P_{d\text{-}max}$ was observed for the optimized MW plasma treatment conditions, which based on ellipsometry measurements carried out with silicon wafer substrates had deposited a carbon layer thickness of 6.4 nm (8.4 %C measured by XPS surface analysis). This enhancement is likely to be due to carbon in the form of graphite with its superior electrical conductivity acting as a charge carrier. This would help to reduce interfacial charge transfer resistance, hence facilitating charge transport and suppressing recombination. As a result, the IPCE response and the short-circuit current density J_{sc} both increased with increasing carbon content up to the 8.4% surface level as highlighted above. At higher levels, the carbon could act as a recombination center as well as a barrier for dye adsorption, both of which led to a decrease in the maximum power density. From this study, it was concluded that the incorporation of carbon onto the surface

of the TiO_2 photoanodes using a microwave plasma during the nanoparticle sintering process can lead to a significant increase in DSSC efficiency.

Acknowledgments

The authors wish to acknowledge the grant of Science Foundation Ireland for funding this work through the Strategic Research Cluster on Solar Energy Conversion (Project No. 07/SRC/B1160). Special thanks to Dr. David Jeng, Dr. Gerald Breen, and Mr. Jonathan Lee of SolarPrint Ltd. for their assistance with this research.

References

[1] M. Grätzel, J. Photochem. Photobiol. C, 4 (2003) 145.
[2] M. Grätzel, Inorg. Chem., 44 (2005) 6841.
[3] M. Grätzel, Acc. Chem. Res., 42 (2009) 1788.
[4] B. O'Regan, M. Grätzel, Nature, 353 (1991) 737.
[5] S.D. Standridge, G.C. Schatz, J.T. Hupp, J. Am. Chem. Soc., 131 (2009) 8407.
[6] H.A. Atwater, A. Polman, Nat. Mater., 9 (2010) 205.
[7] M.D. Brown, T. Suteewong, R.S.S. Kumar, V. D'Innocenzo, A. Petrozza, M.M. Lee, U. Wiesner, H.J. Snaith, Nano Lett., 11 (2011) 438.
[8] S. Guldin, S. Huttner, M. Kolle, M.E. Welland, P. Muller-Buschbaum, R.H. Friend, U. Steiner, N. Tetreault, Nano Lett., 10 (2010) 2303.
[9] S. Colodrero, A. Mihi, L. Haggman, M. Ocana, G. Boschloo, A. Hagfeldt, H. Miguez, Adv. Mater., 21 (2009) 764.
[10] B. Lee, D.K. Hwang, P.J. Guo, S.T. Ho, D.B. Buchholtz, C.Y. Wang, R.P.H. Chang, J. Phys. Chem. B, 114 (2010) 14582.
[11] T.-H. Tsai, S.-C. Chiou, S.-M. Chen, Int. J. Electrochem. Sci., 6 (2011) 3333-3343.
[12] N. Yang, J. Zhai, D. Wang, Y. Chen, L. Jiang, ACS Nano, 4 (2010) 887-894.
[13] Y.H. Jang, X. Xin, M. Byun, Y.J. Jang, Z. Lin, D.H. Kim, Nano Lett., 12 (2012) 479-485.
[14] Y. Saito, S. Matsuda, S. Nogita, J. Mater. Sci. Lett., 5 (1986) 565-568.
[15] Y. Hayashi, T. Tokunaga, T. Soga, T. Jimbo, Y. Yogata, S. Toh, K. Kaneko, Appl. Phys. Lett., 84 (2004) 2886-2888.
[16] S.A. Rakha, G. Yu, J. Cao, S. He, X. Zhou, Diam. Relat. Mater., 19 (2010) 284-287.
[17] M. Awais, M. Rahman, J.M.D. MacElroy, D. Dini, J.G. Vos, D.P. Dowling, Surf. Coat. Tech., 205, Supplement 2 (2011) S245-S249.
[18] A. Dembele, M. Rahman, J.M.D. MacElroy, D.P. Dowling, J. Nanosci. Nanotechnol., 12 (2012) 4769–4774.
[19] Z.S. Wang, H. Kawauchi, T. Kashima, H. Arakawa, Coord. Chem. Rev., 248 (2004) 1381.
[20] K. Hou, B.Z. Tian, F.Y. Li, Z.Q. Bian, D.Y. Zhao, C.H. Huang, J. Mater. Chem., 15 (2005) 2414.

[21] S. Ito, S.M. Zakeeruddin, R. Humphry-Baker, P. Liska, R. Charvet, P. Comte, M.K. Nazeeruddin, P. Péchy, M. Takata, H. Miura, S. Uchida, M. Grätzel, Adv. Mater., 18 (2006) 1202.
[22] S. Ito, T.N. Murakami, P. Comte, P. Liska, C. Grätzel, M.K. Nazeeruddin, M. Grätzel, Thin Solid Films, 516 (2008) 4613.
[23] X. Xin, M. Scheiner, M. Ye, Z. Lin, Langmuir, 27 (2011) 14594.
[24] B.H.Q. Dang, M. Rahman, D. MacElroy, D.P. Dowling, Surf. Coat. Tech., 205 (2011) S235-S240.
[25] B.H.Q. Dang, M. Rahman, D. MacElroy, D.P. Dowling, Surf. Coat. Tech., 206 (2012) 4113-4118.
[26] M.L. McConnell, D.P. Dowling, C. Pope, K. Donnelly, A.G. Ryder, G.M. O'Connor, Diam. Relat. Mater., 11 (2002) 1036-1040.
[27] A.C. Ferrari, J. Robertson, Phys. Rev. B, 61 (2000) 14095-14107.
[28] M. Phaner-Goutorbe, A. Sartre, L. Porte, Microsc. Microanal. M., 5 (1994) 283-290.
[29] V. Ganapathy, B. Karunagaran, S.W. Rhee, J. Power Sources, 195 (2010) 5138-5143.
[30] K.M. Lee, V. Suryanarayanan, K.C. Ho, Sol. Energ. Mat. Sol. C., 91 (2007) 1416-1420.

Figure captions

Fig. 1: XRD spectra of an FTO glass slide (dotted line) and a TiO_2-coated FTO that was sintered with the addition of methane (3.5 sccm) during the MW argon-oxygen plasma treatment.

Fig. 2: Raman spectrum in the range of 100 – 800 cm^{-1} of the TiO_2 sintered with an addition of 3.5 sccm of precursor methane.

Fig. 3: Raman spectra in the range of 900 – 2400 cm^{-1} of the TiO_2 sintered with and without an addition of 3.5 sccm of precursor methane.

Fig. 4: XPS spectrum of C1s state for the TiO_2 sintered with an addition of 3.5 sccm of precursor methane.

Fig. 5: Carbon percentage (%C) and carbon layer thickness for the carbon-incorporated TiO_2 prepared using precursor methane at different flow rates.

Fig. 6: Dye adsorption level and maximum power density ($P_{d\text{-}max}$) measured from the prepared DSSCs as a function of the precursor methane flow rate.

Fig. 7: Open-circuit voltage (V_{oc}) and fill factor (*FF*) measured from the prepared DSSCs as a function of the methane flow rate used in their preparation.

Fig. 8: Short-circuit current density (J_{sc}) measured from the prepared DSSCs as a function of the methane flow rate used in their preparation.

Fig. 9: IPCE responses of TiO_2, 7.9% surface carbon-incorporated, 9.7% surface carbon-incorporated and the best-performing 8.4% surface carbon-incorporated TiO_2 under the illumination of one sun at open-circuit voltage.

Fig. 10: Nyquist plots of the EIS of TiO_2 and the best-performing 8.4% surface carbon-incorporated TiO_2.

Fig. 11: Bode plots of the EIS of TiO_2 and the best-performing 8.4% surface carbon-incorporated TiO_2.

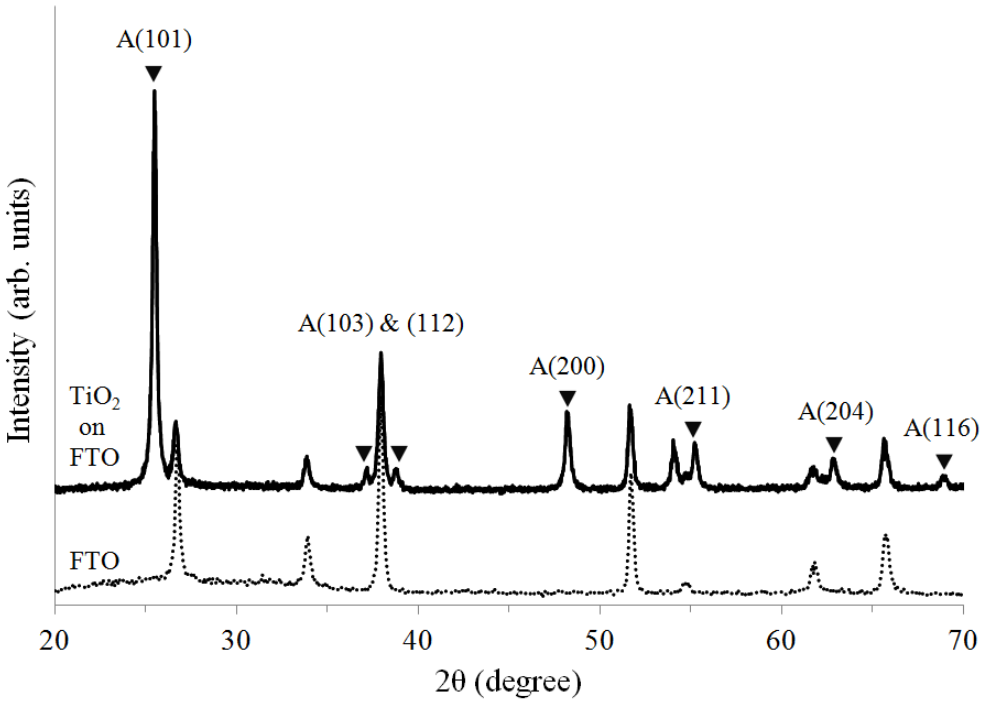
A(101)
A(103) & (112)
A(200)
A(211)
A(204)
A(116)
TiO2 on FTO
FTO
Intensity (arb. units)
20
30
40
50
60
70
2θ (degree)

Fig. 1

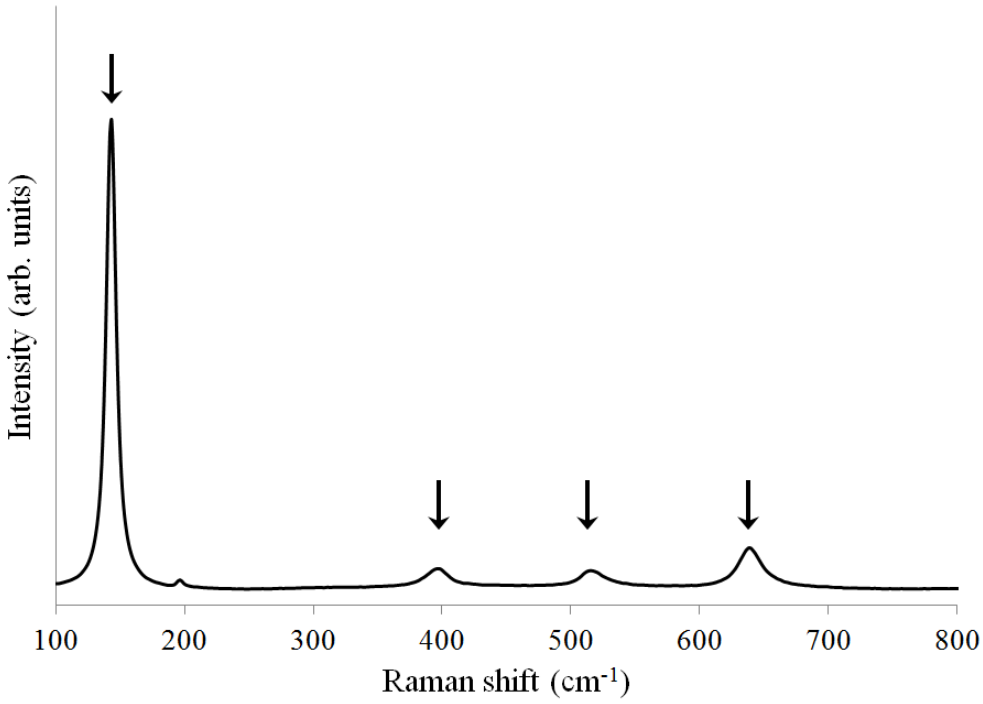
Intensity (arb. units)
100
200
300
400
500
600
700
800
Raman shift (cm-1)

Fig. 2

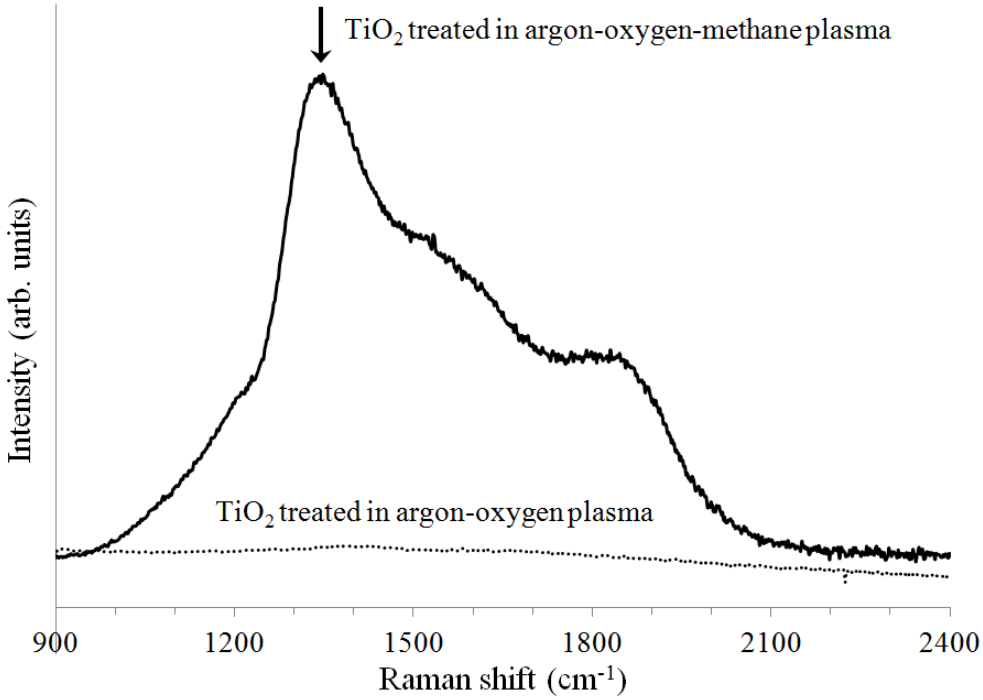
TiO2 treated in argon-oxygen-methane plasma
TiO2 treated in argon-oxygen plasma
Intensity (arb. units)
900
1200
1500
1800
2100
2400
Raman shift (cm-1)

Fig. 3

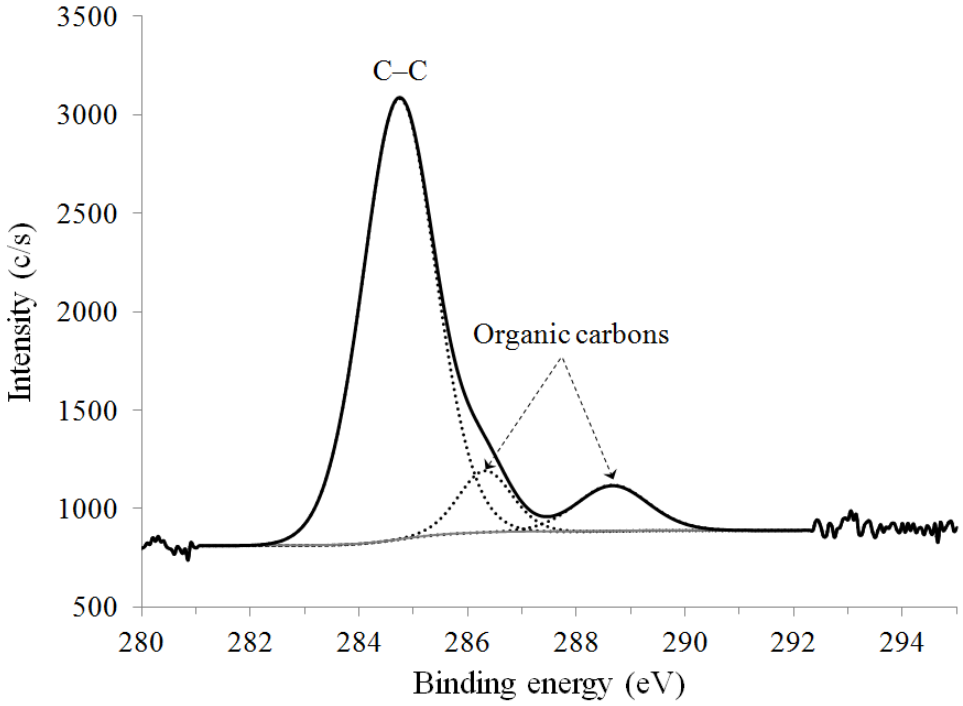
3500
3000
2500
2000
1500
1000
500
Intensity (c/s)
C–C
Organic carbons
280
282
284
286
288
290
292
294
Binding energy (eV)

Fig. 4

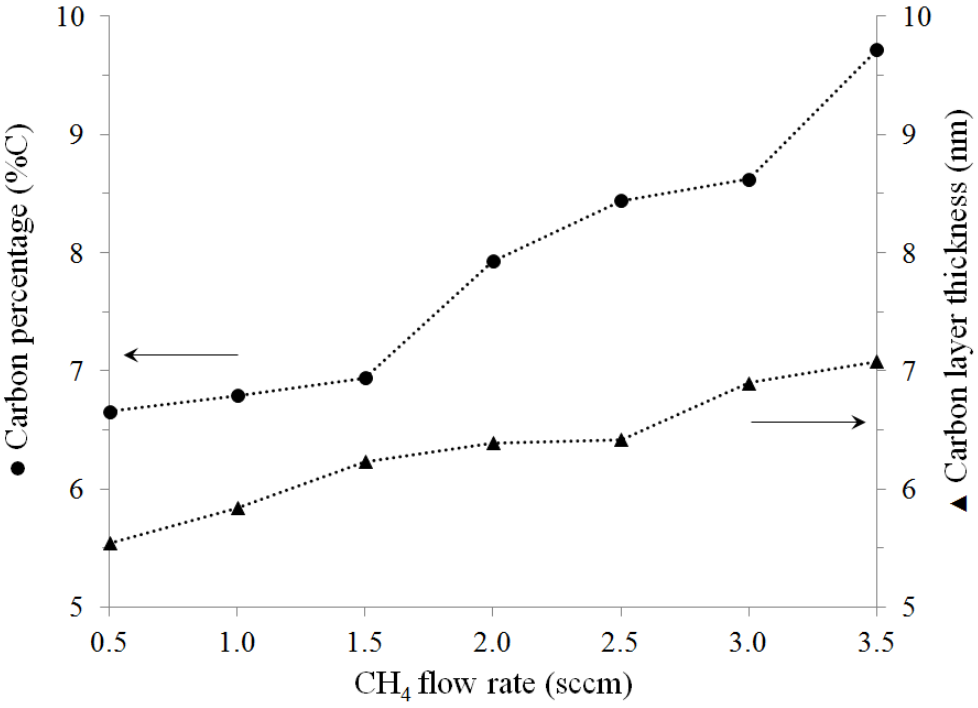
10
9
8
7
6
5
0.5
1.0
1.5
2.0
2.5
3.0
3.5
● Carbon percentage (%C)
▲ Carbon layer thickness (nm)
CH4 flow rate (sccm)

Fig. 5

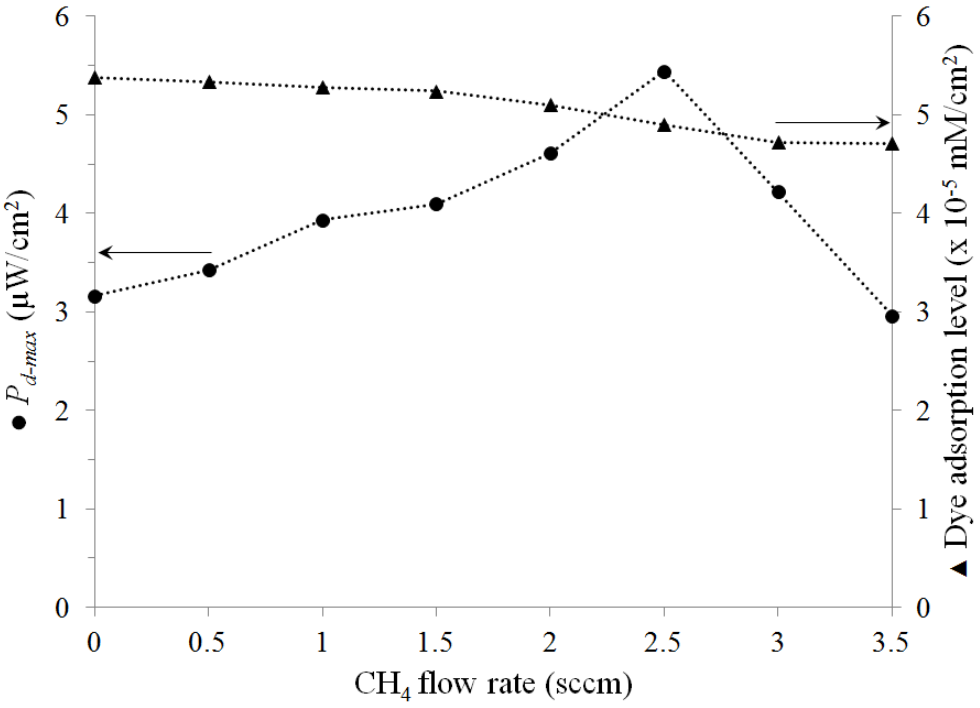
6
5
4
3
2
1
0
0
0.5
1
1.5
2
2.5
3
3.5
● $P_{d\text{-}max}$ (μW/cm²)
▲ Dye adsorption level (x 10⁻⁵ mM/cm²)
CH_4 flow rate (sccm)

Fig. 6

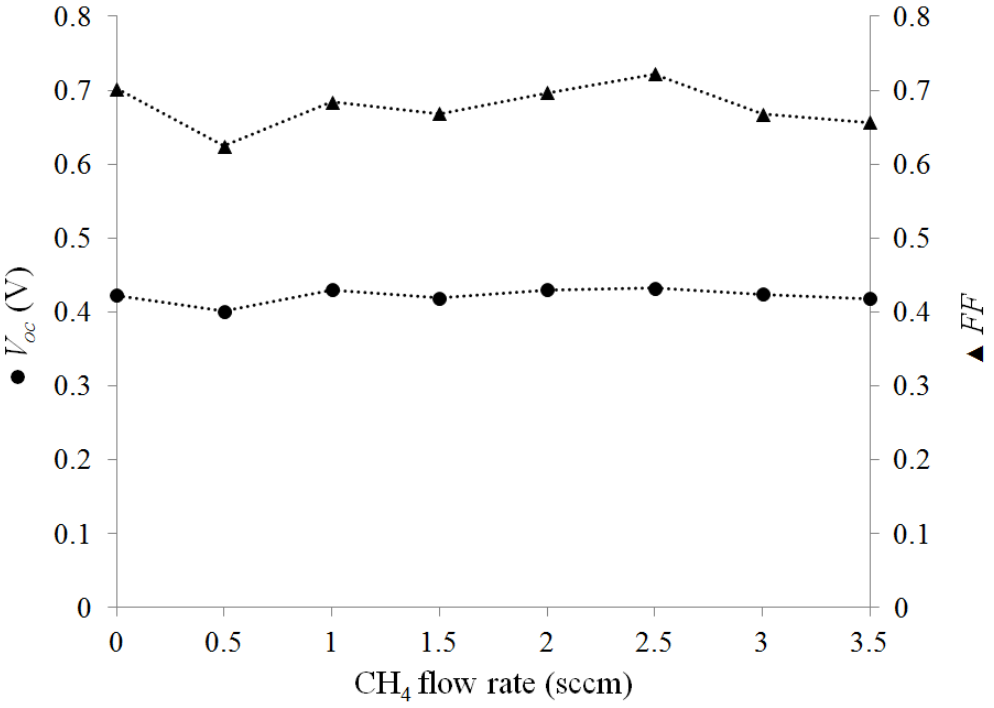
0.8
0.7
0.6
0.5
0.4
0.3
0.2
0.1
0
V_{oc} (V)
FF
0
0.5
1
1.5
2
2.5
3
3.5
CH_4 flow rate (sccm)

Fig. 7

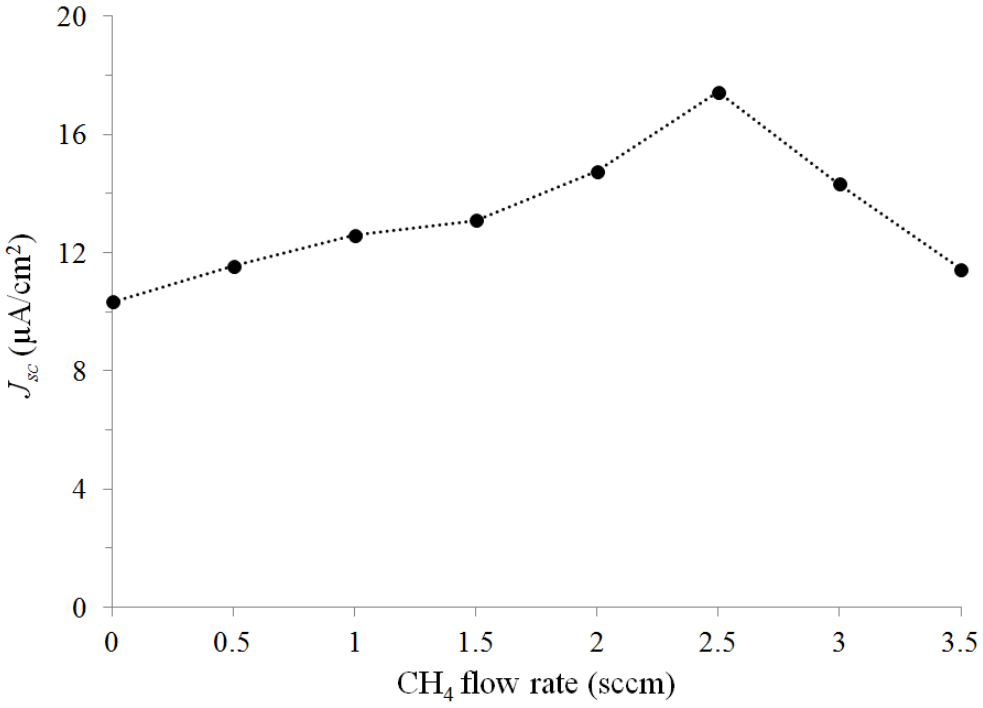

Fig. 8

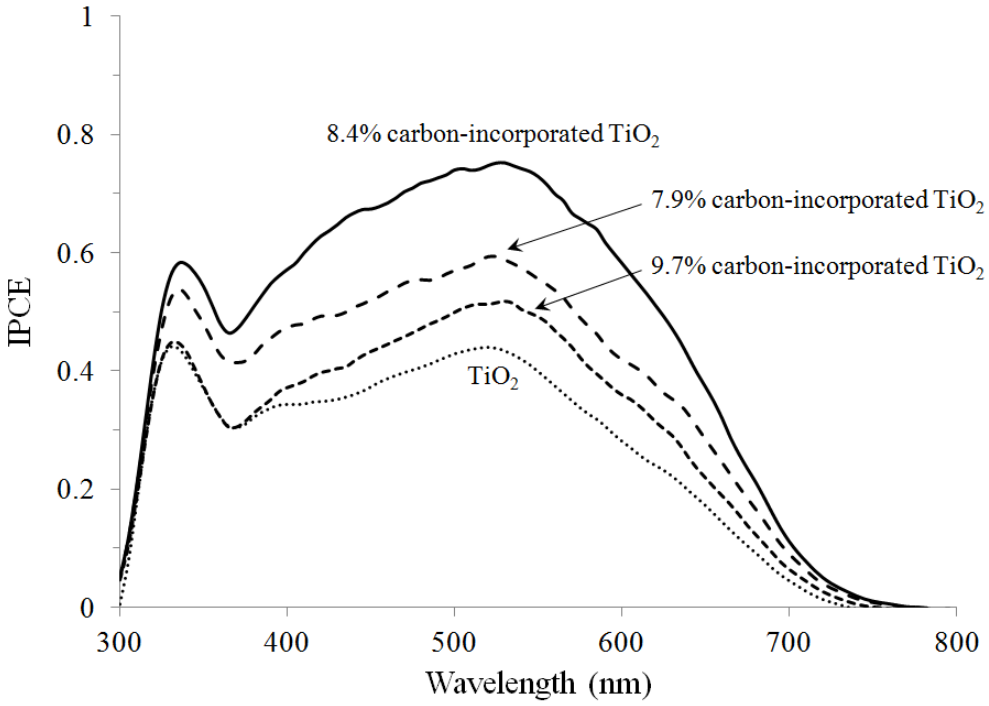
1
0.8
0.6
0.4
0.2
0
IPCE
300
400
500
600
700
800
Wavelength (nm)
8.4% carbon-incorporated TiO2
7.9% carbon-incorporated TiO2
9.7% carbon-incorporated TiO2
TiO2

Fig. 9

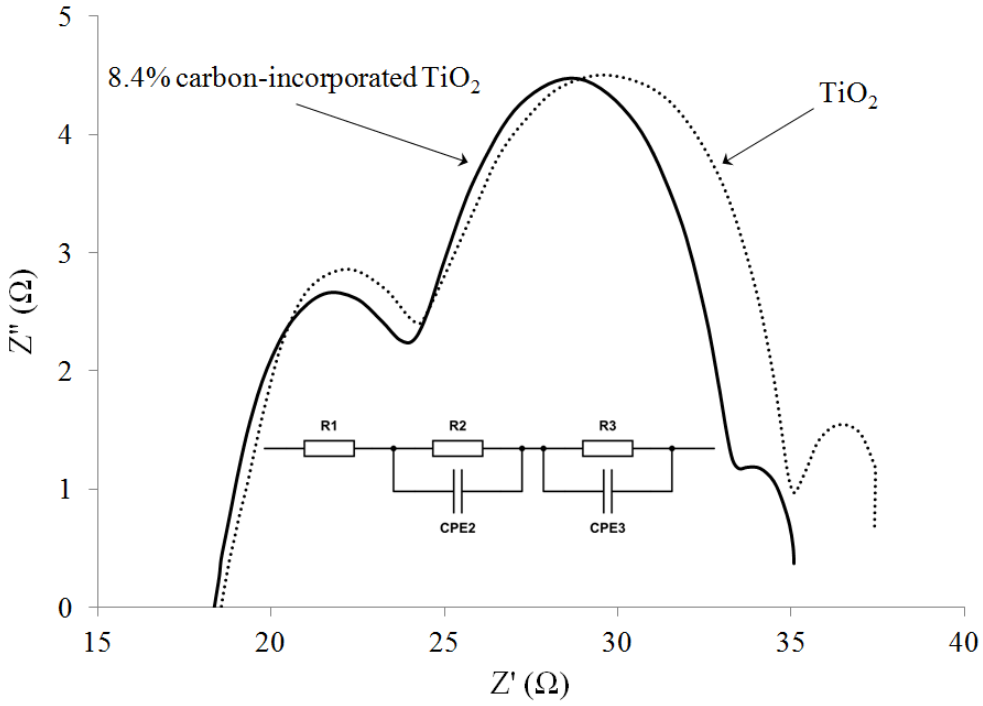
8.4% carbon-incorporated TiO2
TiO2
Z'' (Ω)
Z' (Ω)
R1
R2
R3
CPE2
CPE3
0
1
2
3
4
5
15
20
25
30
35
40

Fig. 10

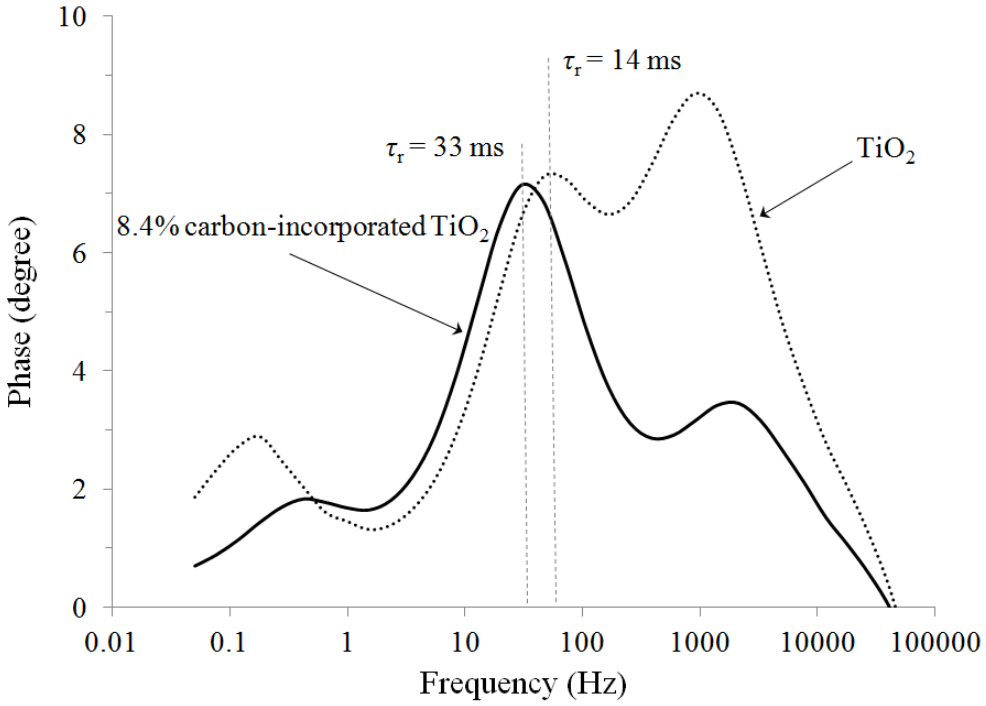
10
8
6
4
2
0
Phase (degree)
τ_r = 14 ms
τ_r = 33 ms
TiO2
8.4% carbon-incorporated TiO2
0.01
0.1
1
10
100
1000
10000
100000
Frequency (Hz)

Fig. 11